Pulsed laser deposition of Bi_2Te_3-based thermoelectric thin films

Raghuveer S. Makala, K. Jagannadham,[a] and B. C. Sales[b]
Department of Materials Science and Engineering, North Carolina State University, Raleigh, North Carolina 27695-7907

(Received 13 February 2003; accepted 25 June 2003)

Thin films of *p*-type $Bi_{0.5}Sb_{1.5}Te_3$, *n*-type $Bi_2Te_{2.7}Se_{0.3}$, and *n*-type $(Bi_2Te_3)_{90}(Sb_2Te_3)_5(Sb_2Se_3)_5$ (with 0.13 wt % SbI_3) were deposited on substrates of mica and aluminum nitride (on silicon) using pulsed laser ablation at substrate temperatures between 300 °C to 500 °C. The films were characterized using x-ray diffraction and transmission electron microscopy for crystalline quality and epitaxial growth on the substrates. The surface morphology and microstructure were examined using scanning electron microscopy. X-ray mapping and energy-dispersive spectroscopy were performed to determine nonstoichiometry in the composition and homogeneity. The quality of the films, in terms of stoichiometric composition and crystal perfection, was studied as a function of growth temperature and laser fluence. The values of the Seebeck coefficient, electrical resistivity, and Hall mobility in the thin films were measured and compared with those in the bulk. Thermoelectric figure of merit of the films was evaluated from the measured parameters. Correlation of the thermoelectric properties, with the crystalline quality and stoichiometric composition of the films, showed the advantages of pulsed laser deposition of the multicomponent thermoelectric thin films. The results illustrate that laser physical vapor deposition is a suitable choice for deposition of multicomponent thermoelectric films. However, optimization of target composition, substrate temperature, and annealing of the films after deposition were found necessary to maintain the desired stoichiometry and low defect density. AlN/Si substrates provided better quality films compared to substrates of mica. Poor adhesion and cracking of the films on mica were found to be detrimental factors. Films deposited on AlN/Si substrates were found to show higher carrier mobility and higher values of Seebeck coefficient. © *2003 American Institute of Physics.*
[DOI: 10.1063/1.1600524]

I. INTRODUCTION

Bi_2Te_3-based compounds with high Seebeck coefficient are well known for use in thermoelectric cooling devices. The crystal structure of these materials is composed of atomic layers in the order of Te/Bi/Te/Te/Bi/Te/Bi/Te/Te/... oriented along the *c* axis with the Te/Te layers held together by weak van der Waal forces.[1] Higher efficiency thin-film thermoelectric devices are widely foreseen to have applications in microelectronics such as heat spreaders for electronic devices and laser diodes. The main benefit of thin-film thermoelectric coolers is the dramatic increase in cooling power density. It has also been established that the use of diamond or an aluminum nitride substrate with high thermal conductivity is necessary to achieve two orders of magnitude higher power density dissipation using the thin-film coolers.[2]

Numerous techniques have been attempted for deposition of thermoelectric films including evaporation, flash evaporation,[3] molecular-beam epitaxy,[4] chemical vapor deposition, sputtering,[5] and laser ablation.[6] A primary difficulty in the deposition of thermoelectric films is maintaining stoichiometry. All the previous studies have reported that the stoichiometry could be achieved only in a small range of substrate temperatures between 250 to 300 °C. Moreover, flash evaporation is difficult to control while hot wall epitaxy is carried out at very high substrate temperatures, thus, restricting the use of many substrates. The problem of resputtering during the film growth is present in sputter deposition while differences in volatility of component elements are present in vacuum evaporation. In addition, cooling the target during sputtering limits the power that can be applied because of the low thermal conductivity of thermoelectric targets. The most important requirement to attain high value for the figure of merit is the stoichiometry in composition within the solubility limits of the phase diagram. A large deviation from stoichiometry arises in vapor deposition because the constituent elements in the target exhibit dissimilar sticking coefficients on the substrate. Also, the tendency for re-evaporation of certain elements from the films is present because of their higher vapor pressure. The ability to replicate the composition of the target material in the film is one of the benefits of pulsed laser deposition (PLD) compared to other thin-film deposition techniques.[7] PLD is preferred over thermal evaporation as the laser-induced expulsion produces a plume of a material with stoichiometry similar to that of the target.[8–12]

We used PLD to deposit thin films from targets of *p*-type $Bi_{0.5}Sb_{1.5}Te_3$, *n*-type $Bi_2Te_{2.7}Se_{0.3}$, and *n*-type $(Bi_2Te_3)_{90}(Sb_2Te_3)_5(Sb_2Se_3)_5$ (with 0.13 wt % SbI_3). These *p*-type and *n*-type compounds are known to be with the op-

[a]Electronic mail: jag_kasichainula@ncsu.edu
[b]Also at: Solid State Division, Oak Ridge National Laboratory, Oak Ridge, TN 37831.

 © 2003 American Institute of Physics

Downloaded 24 Nov 2003 to 160.91.48.189. Redistribution subject to AIP license or copyright, see http://ojps.aip.org/japo/japcr.jsp

timum compositions for fabrication of thermoelectric cooling devices that could be used at room temperature. Highly crystalline and stoichiometric Bi_2Te_3 films have been deposited using PLD.[6] In the present effort, emphasis was given to the deposition of stoichiometric thermoelectric thin films by PLD through variation of deposition parameters such as laser energy, target composition, and substrate characteristics.

II. EXPERIMENT

Substrates of mica and aluminum nitride were chosen to deposit the thermoelectric thin films. Both mica and aluminum nitride are good thermal conductors and possess a hexagonal crystal structure that could be favorable for the Bi_2Te_3-based films with the 00*n* preferred orientation of growth. Moreover, these substrates with a high dielectric constant are also used for heat spreaders in electronic packaging. Because AlN substrates were not readily available, thin films of AlN on silicon (100) and (111) substrates were deposited by dc reactive magnetron sputtering.

A. Preparation of substrates

Thin freshly cleaved mica sheets of 15 μm thickness and AlN on *p*-type Si wafers of 500 μm thickness, with (100) or (111) orientation, were chosen as the substrates. The silicon substrates were cleaned with acetone and methanol to dissolve any contaminants adhering to the surface. Finally, silicon wafers were etched in a 49% hydrofluoric acid solution for about 3 min, followed by rinsing in distilled water, and drying before the deposition of AlN. AlN was sputter deposited on the silicon substrates by a procedure described next.

B. Deposition of aluminum nitride

AlN was deposited on silicon substrates by dc reactive magnetron sputtering in a mixture of ultrahigh-purity argon and nitrogen gases.[13,14] The partial pressures of argon and nitrogen were both maintained between 0–1 mTorr in the deposition chamber with a total sputtering pressure of 2–3 mTorr. A high-purity aluminum (99.999%) disk, 100 mm in diameter, was used as a target with a pulsed dc power source. The stainless-steel deposition chamber was evacuated to a predeposition vacuum of 5×10^{-6} Torr using a turbomolecular pump backed by a rotary pump. The substrate temperature was raised to 600 °C by a resistance heater. Initially, argon was introduced to a partial pressure of 0–1 mTorr and plasma generated at a target current of 0.5 A for sputter cleaning the target surface for 2 min. A movable shutter was used to mask the substrates during this stage. The target current was increased to 2 A while ultrapure nitrogen gas was introduced to a partial pressure of 0–1 mTorr into the chamber. At this juncture, the ratio of circulating power to effective power was found to be between 0.62 and 1.05. This value of the ratio was indicative of the insulating nature of the AlN film that is formed during deposition. The deposition was carried out for 60 min.

C. Pulsed laser deposition of thermoelectric thin films

The $Bi_{0.5}Sb_{1.5}Te_3$ (*p*-type) target for PLD was made by sintering the powder compacts. The $Bi_2Te_{2.7}Se_{0.3}$ and $(Bi_2Te_3)_{90}(Sb_2Te_3)_5(Sb_2Se_3)_5$ $(+0.13\,\text{wt}\,\%\ SbI_3)$ (*n*-type) ingots were grown by the Bridgman method and the targets were obtained by slicing the ingots with a diamond saw perpendicular to the growth axis to yield smaller circular disks of 25 mm in diameter and 10 mm in thickness. The same targets were used for the deposition of several films. The target was loaded in a stage that was rotated about the normal to the surface. Either mica or AlN/Si(100) or AlN/Si(111) substrates were loaded in the stainless-steel vacuum chamber. The center of the target coincided approximately with the center of the substrate and was separated by 4 cm. The substrate was heated with a tungsten bulb heater. The deposition chamber was evacuated to 1×10^{-7}–5×10^{-7} Torr by a turbomolecular pump backed by a rotary pump. The substrate was heated to a temperature between 300 °C and 500 °C for various depositions. The temperature of the substrate was measured by placing a thermocouple on a Si sample close to substrate of deposition and placed on the heater plate covering the tungsten bulb. The temperature of the substrate was allowed to reach a stable value by allowing sufficient time before deposition.

A pulsed Nd–YAG laser operating at 10 Hz frequency and delivering the fourth harmonic ($\lambda=266$ nm, pulse duration: $\tau=8$–9 ns) was used to ablate the target. The laser beam was focused onto the target with a converging lens of 50 mm focal length. The laser beam was incident on the target at 45°. A schematic of our experimental PLD setup is illustrated in Fig. 1. The target was rotated to avoid nonstoichiometry resulting from localized evaporation from the same region in the target. The laser-generated plume was deposited on the substrate. The laser fluence was also controlled by means of tuning the harmonic generators to a maximum energy of 0.25 J/cm^2. The pressure in the deposition chamber was found to change from 8×10^{-7} to 7×10^{-6} Torr during the deposition upon increase in laser energy to the maximum value. The deposition time was also varied between 30 min and 1 h to increase the thickness of the film. In addition, the films on AlN/Si substrates were deposited at a lower laser fluence of 0.18 J/cm^2 and were subsequently annealed *in situ* at 200 °C in the deposition chamber for 2 h. During annealing, the vacuum level in the chamber was the same as that obtained prior to the deposition. The laser fluence, substrate temperature, time of deposition, and substrate orientation were varied in the deposition of different films. However, all the depositions on AlN/Si substrates were carried out at lower laser fluence that resulted in lower particulate emission in the plume. The thickness of the films measured by a profilometer was found to be 1.5 μm for a deposition time of 1 h. Thus, the deposition rate of 0.4 nm/s was observed.

Downloaded 24 Nov 2003 to 160.91.48.189. Redistribution subject to AIP license or copyright, see http://ojps.aip.org/japo/japcr.jsp

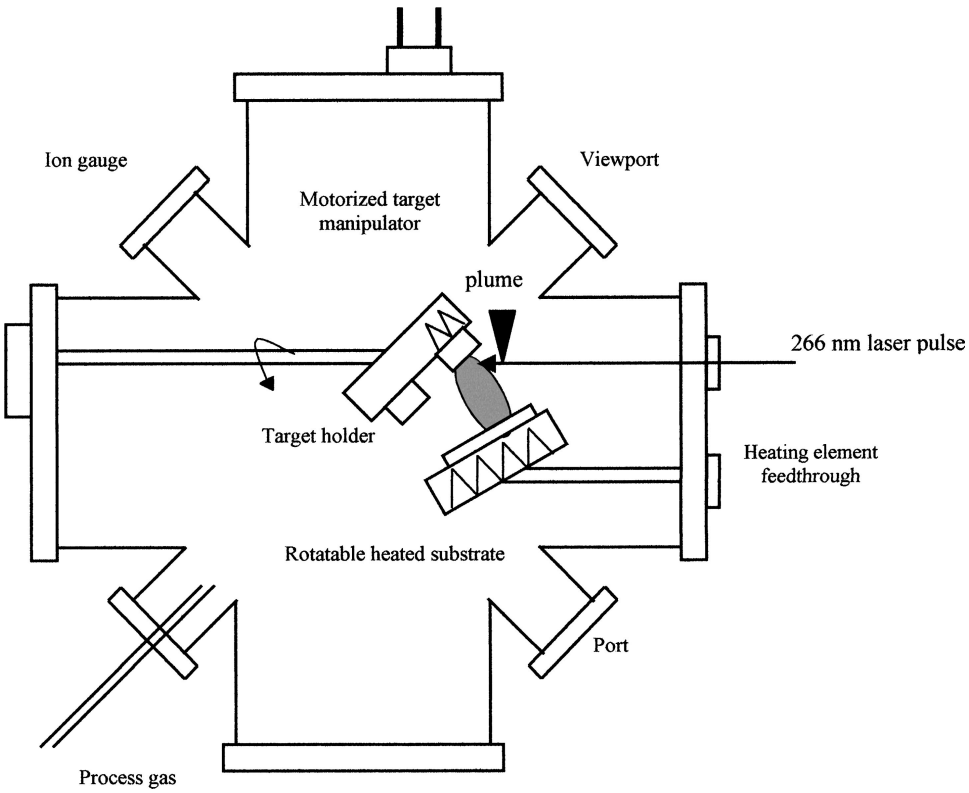

FIG. 1. Schematic of PLD setup used for deposition of thermoelectric films.

III. RESULTS

A. X-ray diffraction

A Rigaku diffractometer was used for x-ray diffraction analysis and θ–2θ scans were obtained using nickel-filtered Cu $K\alpha$ radiation ($\lambda = 0.154\,06$ nm) at an accelerating voltage of 27.5 kV and an anode current of 20 mA. The diffraction patterns from the films deposited on mica at 350 °C are shown in Figs. 2(a)–2(c). Mica available in different forms is pseudohexagonal with $a = 0.5199$ nm, $b = 0.9027$ nm, and $c = 2.0106$ nm. $Bi_{0.5}Sb_{1.5}Te_3$ belongs to trigonal system with an equivalent hexagonal unit cell given by $a = 0.4401$ nm and $c = 2.7187$ nm. Similarly, the hexagonal unit cell of $Bi_2Te_{2.7}Se_{0.3}$ is given by $a = 0.4266$ nm and $c = 2.985\,51$ nm. It must be pointed out that because of the variations in the composition of these compounds, the values of the lattice parameters are obtained from the indexed reflections shown in Figs. 2(a)–2(c). The observed reflections illustrate preferential growth along the c axis. The $(003n)$ family of peaks belongs to the thermoelectric film and the peaks from mica substrate are designated by $m(002p)$. Here, n and p are positive integers that take values from 3 to 8. For every $m(002p)$ peak arising from the mica substrate, a $(003n)$ peak corresponding to the film was also observed. This result confirms that the films were well textured, if not epitaxial. In addition, low intensity peaks corresponding to reflections such as (0111), (205), and (0210) were also present in the n-type films. The results of x-ray diffraction from p and n-type thermoelectric films deposited on AlN/Si(100) and AlN/Si(111) are shown in Figs. 3(a)–3(c) respectively. The crystal structure of AlN is hexagonal with $a = 0.3114$ nm and $c = 0.4979$ nm. It is seen that the peaks corresponding to strong reflections from only (006), (009), and (0012) planes were present, in addition to that of the reflections from silicon and AlN, and thus indicate highly textured or epitaxial growth along the c axis. Certain low intensity reflections were found to arise from half wavelength value of the characteristic Cu $K\alpha$ (0.154 06 nm) in the continuous spectrum that was not effectively filtered. However, the presence of low index reflections and low intensity high-order reflections is observed in the films deposited on AlN/Si. The absence of other reflections from the film deposited on AlN/Si is further taken as improvement in the textured growth.

B. Scanning electron microscopy

The growth morphology and composition of thermoelectric thin films deposited on mica and AlN were characterized using a Hitachi S-3200 scanning electron microscope (SEM), as shown in Figs. 4(a) and 4(b). An accelerating voltage of 10 kV was applied and a magnification ranging from 100× to 7000× was used to examine the morphology of the films. The images from the films deposited at a substrate temperature of 350 °C showed the presence of particulates that were indicative of higher deposition rates and higher laser energy. Two types of particulates were observed: (1) Micron or submicron droplets and (2) larger particulates shaped like flat disks. The formation of larger particulates in the films deposited on AlN/Si was reduced at lower laser fluence. SEM micrographs shown in Fig. 4(b) clearly illustrate the reduction in particulate density in the films deposited at lower laser fluence.

X-ray maps were obtained to determine the distribution of different elements in the films. The x-ray maps of different elements in n-type films on mica are shown in Fig. 5. These

Downloaded 24 Nov 2003 to 160.91.48.189. Redistribution subject to AIP license or copyright, see http://ojps.aip.org/japo/japcr.jsp

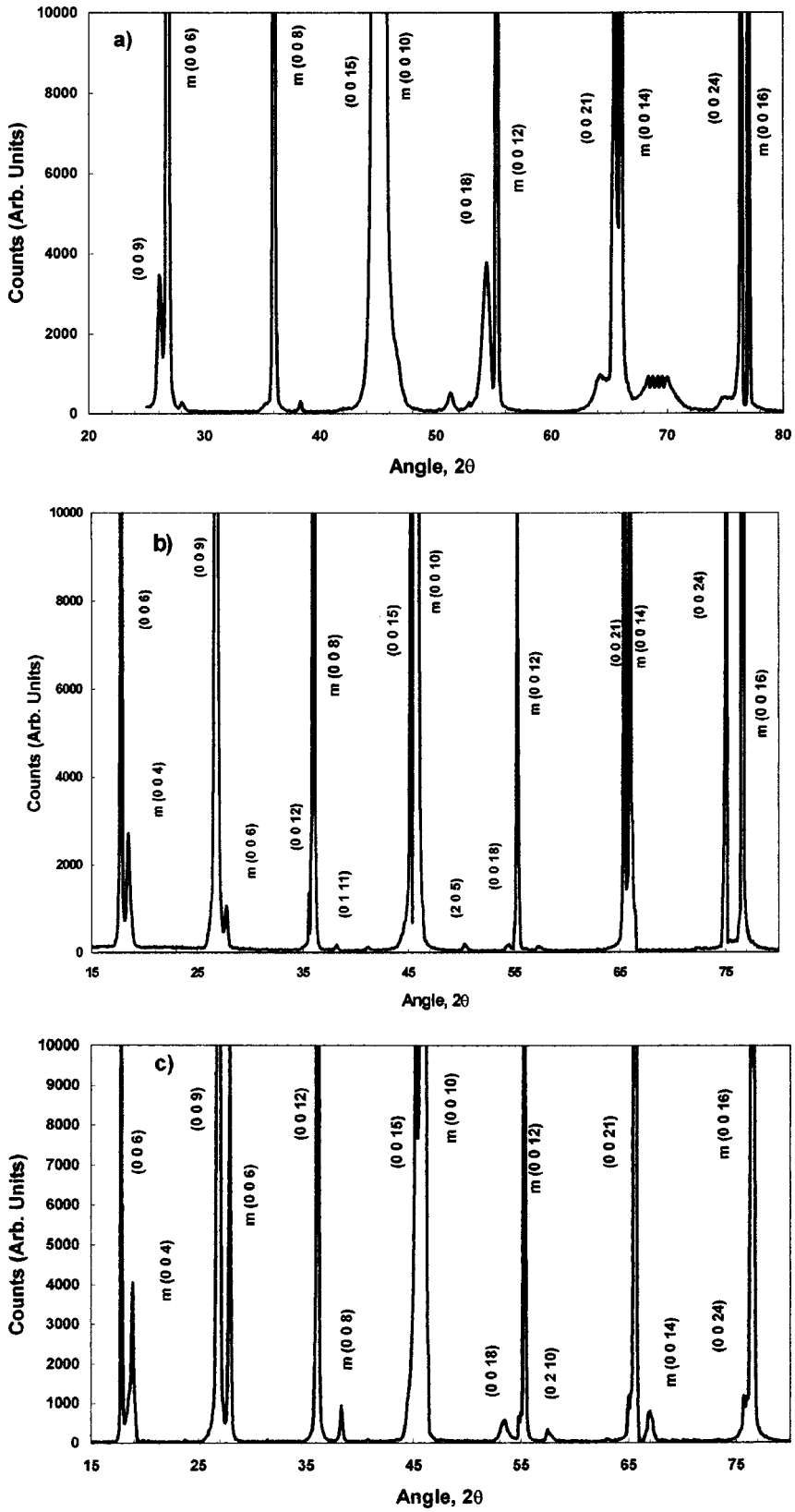

FIG. 2. (a) θ–2θ x-ray diffraction scan obtained on $Bi_{0.5}Sb_{1.5}Te_3$ thin films deposited on mica. (b) θ–2θ x-ray diffraction scan obtained on $Bi_2Te_{2.7}Se_{0.3}$ thin films deposited on mica. (c) θ–2θ x-ray diffraction scan obtained on thin films deposited on mica substrates using a $(Bi_2Te_3)_{90}(Sb_2Te_3)_{10}(Sb_2Se_3)_{10}$ $(+0.13\,\text{wt}\,\%\ SbI_3)$ target.

maps were obtained from same regions, as shown in the SEM images. Figure 5 illustrates the presence of the elements bismuth, tellurium, and selenium in the film, in addition to those from the substrate. Energy-dispersive spectroscopy (EDS) was also performed for quantitative analysis of different elements in both the *n*- and *p*-type thin films and the respective targets and the results are summarized in Table I. It was noted that all the films compared to the targets were deficient in tellurium. Tellurium has higher vapor pressure among the elements in the target. Furthermore, compared to the films on mica those on aluminum nitride were closer to the target stoichiometry, as seen from the results listed in the

Downloaded 24 Nov 2003 to 160.91.48.189. Redistribution subject to AIP license or copyright, see http://ojps.aip.org/japo/japcr.jsp

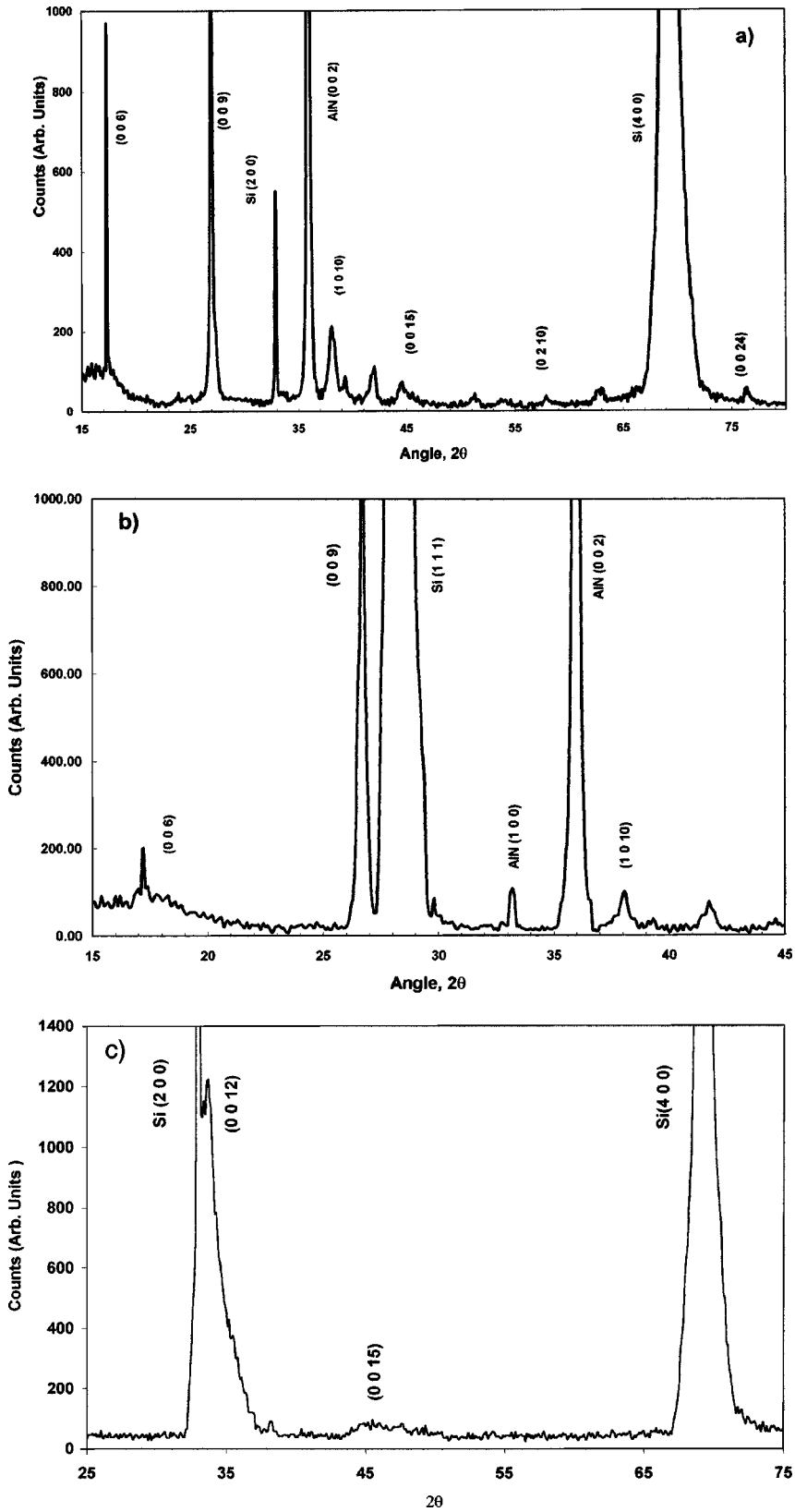

FIG. 3. (a) θ–2θ x-ray diffraction scan obtained on $Bi_{0.5}Sb_{1.5}Te_3$ thermoelectric thin films deposited on AlN/Si(100) substrate. (b) θ–2θ x-ray diffraction scan obtained on $Bi_{0.5}Sb_{1.5}Te_3$ thermoelectric thin films deposited on AlN/Si(111) substrate. (c) θ–2θ x-ray diffraction scan obtained on $(Bi_2Te_3)_{90}(Sb_2Te_3)_{10}(Sb_2Se_3)_{10}$ $(+0.13\,\text{wt}\,\%\ SbI_3)$ thermoelectric thin films deposited on AlN/Si(100) substrate.

Table I. The analysis also showed that the composition of the particulates was very much similar to that of the film. The results of quantitative analysis of films deposited on AlN with improved predeposition vacuum of 1×10^{-7} Torr showed a slight improvement in the composition towards that of the target.

C. Transmission electron microscopy

Plan-view samples of thermoelectric thin films deposited on mica were examined in a TOPCON EM002B microscope at an accelerating voltage of 200 kV, with spherical aberration, $C_s = 0.5$ mm, and 0.18 nm point-to-point, and 0.12 nm

Downloaded 24 Nov 2003 to 160.91.48.189. Redistribution subject to AIP license or copyright, see http://ojps.aip.org/japo/japcr.jsp

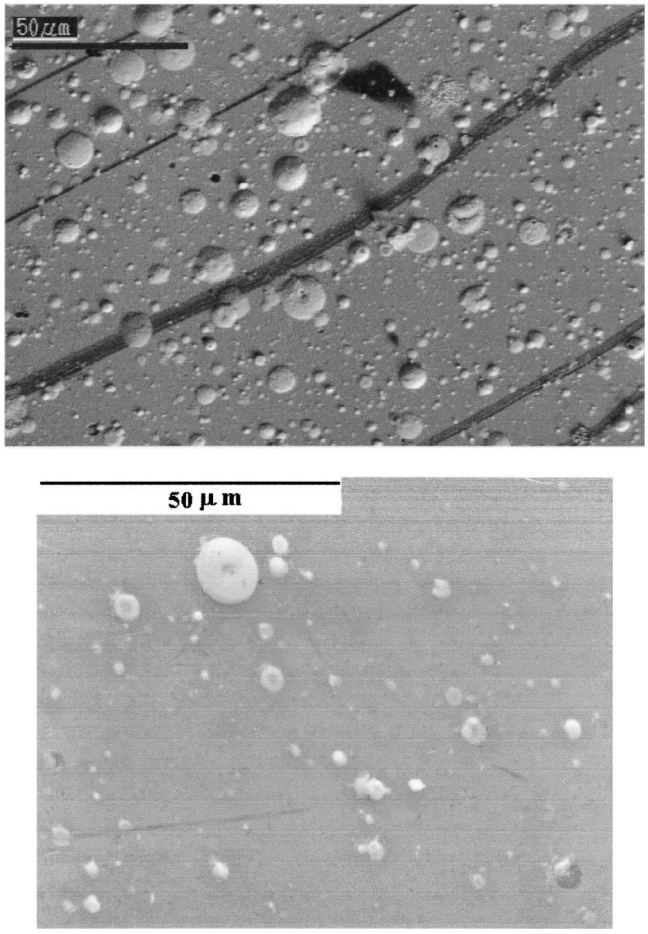

FIG. 4. (a) SEM micrograph obtained on *n*-type films deposited on mica substrates using high incident laser fluence. (b) SEM micrograph obtained on *n*-type films deposited on AlN substrates using low incident laser fluence.

line-to-line resolution. The selected area diffraction pattern (SADP) from the mica substrate is shown in Fig. 6(a) and illustrates the reflections obtained from the [0001] hexagonal zone axis. The SADP obtained from the thermoelectric film on mica substrate is shown in Fig. 6(b). The satellite spots, in addition to those obtained for mica, arise from the reflections that belong to the thermoelectric film. This is indicative of preferred growth of the film along the *c* axis of the substrate. A transmission electron microscopy (TEM) bright-field image of the film is shown in Fig. 6(c). Hexagonal crystallites that were oriented with the *c* axis perpendicular to the plane of the substrate were seen.

D. Transport properties

Seebeck coefficient (thermopower) was measured on all the films as a function of temperature difference dT and the observed values are shown in Tables II(a) and II(b) for films deposited on mica and AlN/Si substrates, respectively. Table II(c) provides the values of the Seebeck coefficient for films deposited on AlN/Si(100) with better predeposition vacuum. The mobility and carrier concentration were not measured in these films deposited with better predeposition vacuum. The highest values of the measured Seebeck coefficient, mobility, and carrier concentration are listed in Table III. Higher values were obtained on *n*-type films deposited at 350 °C and on *p*-type films deposited at 300 °C. The Seebeck value was -224.51 μV/K for the *n*-type $Bi_2Te_{2.7}Se_{0.3}$ bulk target. In comparison, a value of -74.15 μV/K (see Table II) was found in the best *n*-type film on mica deposited from the $(Bi_2Te_3)_{90}(Sb_2Te_3)_5(Sb_2Se_3)_5$ target at a substrate temperature of 350 °C. The Seebeck coefficient for the *p*-type $Bi_{0.5}Sb_{1.5}Te_3$ bulk target was only 40.52 μV/K. As mentioned previously, the *p*-type target was processed by sintering the powder compact and the lower value of Seebeck coefficient could be attributed to nonuniform composition resulting from incomplete sintering. Compared to this lower value, the highest Seebeck coefficient in the *p*-type film deposited on mica was 86.64 μV/K. The value of Seebeck coefficient could not be experimentally determined from the *n*-type $(Bi_2Te_3)_{90}(Sb_2Te_3)_5(Sb_2Se_3)_5$ target as its dimensions were too small. The thermoelectric thin films deposited on AlN/Si, however, showed larger values of thermopower compared to the films on mica. The *n*-type film on AlN/Si showed a Seebeck value of -154.69 μV/K while a value of 142.2 μV/K was found in the *p*-type film, both deposited at 350 °C. The improved values of thermopower are related to the use of lower incident laser fluence and the inclusion of an additional annealing step for 2 h at 200 °C. The results summarized in Table II(c) illustrate an improvement in thermopower for the films deposited on AlN/Si(100). The changes in the quality of the films upon annealing as seen in the results of x-ray diffraction were not significant but the

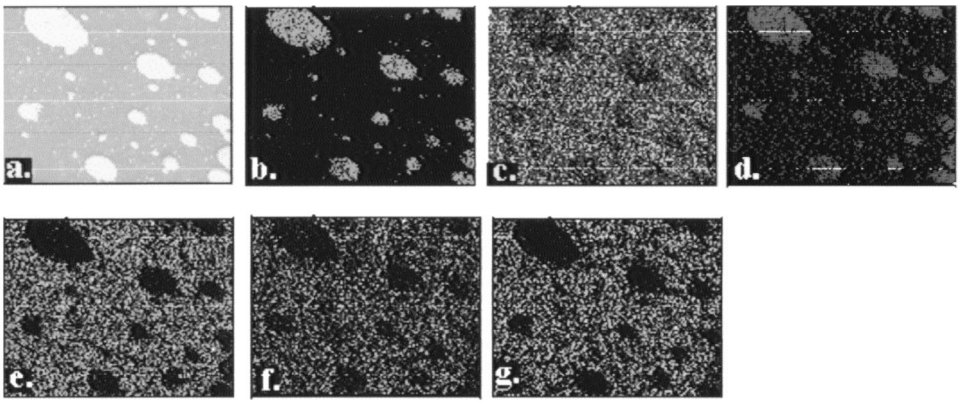

FIG. 5. X-ray map of micrograph obtained on *n*-type $Bi_2Te_{2.7}Se_{0.3}$ films deposited on AlN substrates using a high incident laser fluence. Image is shown in (a), Bi in (b), Se in (c), Te in (d), Si in (e), Al in (f), and N in (g).

Downloaded 24 Nov 2003 to 160.91.48.189. Redistribution subject to AIP license or copyright, see http://ojps.aip.org/japo/japcr.jsp

TABLE I. Composition analysis of films deposited at 350 °C using EDS.

			Films on mica			Films on AlN/Si(100)			Films on AlN/Si(100) deposited at base pressures of 1×10^{-7} Torr		
	Element	Target	Overall	Particulates	Film	Overall	Particulates	Film	Overall	Particulates	Film
p-$Bi_{0.5}Sb_{1.5}Te_3$	Bi	11.57	12.48	11.35	13.2	11.18	10.32	11.55	11.06	10.12	11.81
	Sb	29.18	36.97	38.47	35.68	34.47	36.18	30.47	30.69	30.85	30.03
	Te	59.25	50.55	49.08	51.11	57.35	58.5	57.98	58.13	59.03	58.16
n-$(Bi_2Te_3)_{90}(Sb_2Te_3)_5(Sb_2Se_3)_5$ (0.13 wt % SbI_3 doped)	Bi	27.48	32.01	31.35	32.75	30.26	29.72	31.14	28.59	29.18	28.44
	Sb	13.71	17.13	16.81	19.14	13.26	13.34	12.03	14.27	14.34	14.32
	Te	55.9	49.12	49.86	46.57	53.54	53.42	54.58	54.05	53.78	54.27
	Se	2.55	1.13	1.02	1.18	2.58	2.67	2.09	2.64	2.18	2.51
	I	0.35	0.61	0.96	0.24	0.36	0.85	0.16	0.42	0.31	0.46
n-$Bi_2Te_{2.7}Se_{0.3}$	Bi	39.62	46.24	46.81	47.39	42.94	43.01	42.74	42.48	41.02	41.68
	Te	54.44	46.16	48.06	48.77	51.72	51.01	51.43	52.39	53.78	52.63
	Se	5.94	7.43	5.08	4.3	5.31	5.98	5.83	5.08	5.17	5.69

transport properties were improved. We believe that annealing the point defects contributed to the improvement via reduced scattering and increase in the mobility of the carriers. Results presented in Tables II(a)–II(c) and III may be correlated with the Seebeck value taken as the label for each sample. These results allow us to conclude that the value of the Seebeck coefficient remained higher when the mobility of the carriers was also higher or close to the highest value.

Measurements were made on all the films to determine Hall mobility and carrier concentration, and again the highest values are shown in Table III. Specifically, while carrier concentration should be optimized, the results of higher mobility are given importance with the carrier concentration in the same film provided. The films deposited from the SbI_3 doped target showed higher Seebeck coefficient and higher mobility. Better n-type films were obtained at a substrate temperature of 350 °C whereas better p-type films were obtained at 300 °C on the mica. The highest carrier mobility in the films on mica was 40.42 $cm^2/V\,s$ for the n-type deposited at 350 °C with SbI_3 doping and 28.89 $cm^2/V\,s$ for p-type deposited at 300 °C. The value of mobility improved to 68.84 $cm^2/V\,s$ on the n-type films (with SbI_3 doping) deposited on AlN/Si(111) at 350 °C. The resistivity in this particular film, provided in Table II(b), was found to be $9.48\times10^{-3}\ \Omega$ cm. Better transport properties were observed in the films deposited on AlN/Si(100) compared to those on AlN/Si(111).

IV. DISCUSSION

Cleaved mica substrates provide the hexagonal in-plane symmetry with large and atomically smooth surfaces and were chosen as the substrate materials for the deposition of the thermoelectric thin films. The Bi_2Te_3-based thermoelectric compounds are expected to crystallize in a hexagonal structure with the growth oriented along the c axis. The presence of the (003) family of peaks in the x-ray diffraction patterns illustrates deposition of textured films with growth along the c axis. However, the limited adhesion of the films and presence of cleavage steps on mica substrates necessitated the use of AlN/Si substrates with (0001) preferred crystallographic orientation of AlN. Growth of $(003n)$ oriented films is encouraged by the hexagonal atomic arrangement present in mica and AlN. However, the in-plane crystallographic growth relationship in terms of atomic arrangement has not been determined in the present work.

Characterization of the thermoelectric films by SEM revealed uniform deposition, however, with the presence of particulates. Particulates are considered to form as a result of surface roughening followed by shock wave recoil from the target. The incident laser beam produces microscopic irregularities on the target surface. The laser-induced thermal and mechanical shock waves dislodge and eject particles from the surface irregularities in the form of molten micron-sized globules that are deposited on the substrate. The films with the surface morphology, shown in the SEM micrographs in Fig. 4(a), were deposited at incident energy of 0.25 J/cm^2. The density of the particulates was reduced but not completely eliminated upon lowering the laser fluence to 0.125 J/cm^2, as shown in Fig. 4(b).

X-ray maps are useful for the qualitative analysis of the distribution of the elements in the film. Results of quantitative analysis of the composition of the films using EDS are presented in Table I. The uniform distribution of all of the elements and absence of preferential segregation along grain boundaries in the films is inferred from the results shown in Fig. 5. From results shown in Table I, it is concluded that the particulates shown in Fig. 5 are richer in bismuth and tellurium. Tellurium has a higher vapor pressure among the constituents in the target and the formation of tellurium rich particulates suggests that these are dislodged from the target without further evaporation during PLD. On the other hand, we have observed tellurium deficiency in the films deposited on mica. The analysis also showed that the composition of the particulates is very much similar to that of the film. The interaction between the higher incident laser energy and target surface is expected to raise the temperature so that tellurium is preferentially depleted by evaporation from the target surface.[15,16] Continuous laser ablation from the same region on the target surface increases the tellurium deficiency and, therefore, the film is also deficient in tellurium. However, the

Downloaded 24 Nov 2003 to 160.91.48.189. Redistribution subject to AIP license or copyright, see http://ojps.aip.org/japo/japcr.jsp

TABLE II. (a). Values of Seebeck coefficient, carrier mobility, and carrier concentration in the thermoelectric films deposited on mica.

Films deposited on mica	Substrate deposition temperature (°C)	Seebeck coefficient (μV/K)	Hall effect measurements		
			Resistivity ρ(ohm cm)	Hall mobility (cm^2/V s)	Carrier Concentration (/cc)
p-$Bi_{0.5}Sb_{1.5}Te_3$	300	86.64	1.04×10^{-2}	26.32	3.31×10^{18}
	350	37.74	2.58×10^{-2}	15.45	1.56×10^{19}
	400	49.76	8.01×10^{-3}	22.84	3.41×10^{19}
	450	49.00	3.9×10^{-2}	20.09	8.59×10^{18}
	500	34.65	1.16×10^{-2}	28.89	1.87×10^{19}
n-$Bi_2Se_{2.7}Te_{0.3}$	300	−31.10	1.69×10^{-3}	27.22	1.38×10^{20}
	350	−53.47	1.71×10^{-3}	35.37	1.21×10^{20}
	400	−45.04	2.85×10^{-3}	24.97	9.86×10^{19}
n-$(Bi_2Te_3)_{90}(Sb_2$	300	−30.80	1.39×10^{-3}	14.43	3.24×10^{19}
$Te_3)_5(Sb_2Se_3)_5$	350	−74.15	5.06×10^{-3}	40.42	2.63×10^{19}
(SbI_3 doped)	400	−49.13	5.03×10^{-3}	38.34	3.61×10^{19}

(b). Values of Seebeck coefficient, carrier mobility, and carrier concentration in the thermoelectric films deposited on AlN/Si.

Films deposited on AlN		Substrate deposition temperature (°C)	Seebeck coefficient (μV/K)	Hall effect measurements		
				Resistivity ρ(ohm cm)	Hall mobility (cm^2/V s)	Carrier Concentration (/cc)
$Bi_{0.5}Sb_{1.5}Te_3$ films	AlN/	300	104.51	1.79×10^{-2}	29.07	9.89×10^{18}
	Si(100)	350	142.20	1.94×10^{-2}	35.33	1.02×10^{19}
	AlN/	300	96.37	1.86×10^{-2}	15.48	4.46×10^{19}
	Si(111)	350	124.34	2.05×10^{-2}	19.41	1.28×10^{19}
n-$Bi_2Se_{2.7}Te_{0.3}$	AlN/	300	−77.52	3.41×10^{-3}	41.37	1.39×10^{20}
	Si(100)	350	−54.89	1.86×10^{-3}	33.98	2.15×10^{20}
	AlN/	300	−43.71	1.26×10^{-3}	24.63	1.78×10^{20}
	Si(111)	350	−28.91	1.27×10^{-3}	13.74	3.59×10^{20}
n-$(Bi_2Te_3)_{90}(Sb_2Te_3)_5(Sb_2Se_3)_5$ (SbI_3 doped)	AlN/	300	−147.64	9.43×10^{-3}	65.37	1.3×10^{19}
	Si(100)	350	−104.15	5.06×10^{-3}	40.42	5.63×10^{19}
	AlN/	300	−62.94	3.69×10^{-3}	36.29	4.43×10^{19}
	Si(111)	350	−154.69	9.48×10^{-3}	68.84	9.58×10^{18}

(c). The values of Seebeck coefficient and electrical resistivity in the films deposited on AlN/Si(100) substrates at a predeposition vacuum of 1.0×10^{-7} Torr.

Films deposited on AlN/Si(100)	Seebeck coefficient (μV/K)	Resistivity, ρ(ohm cm)
$Bi_{0.5}Sb_{1.5}Te_3$	138.42	1.13×10^{-2}
$Bi_2Se_{2.7}Te_{0.3}$	−81.32	1.23×10^{-3}
n-$(Bi_2Te_3)_{90}(Sb_2Te_3)_5(Sb_2Se_3)_5$ (0.13 wt % SbI_3 doped)	−166.37	1.17×10^{-2}

composition of the films deposited on AlN/Si at lower incident laser energy is closer to the target stoichiometry and also showed less variation between the particulates and the film. This result is explained by the lower temperature attained by the target surface at lower laser energy. In addition, EDS analysis of films deposited on AlN under better predeposition vacuum (1×10^{-7} Torr) showed a further improvement in composition toward that of the target. The reduction of oxygen in the chamber for improved vacuum prevents formations of oxides in the laser-generated plume and enables tellurium to reach the substrate. Thus, a nearly congruent transfer of target stoichiometry was achieved by the generation of a plume at lower laser fluences and a better predeposition vacuum.

The microstructure of the films is very important as grain boundaries and crystalline defects increase the resistivity by scattering the charge carriers.[15] The mean-free path of carriers in the films evaluated from conductivity and carrier concentration is found to be between 5 to 15 nm and thus grain boundaries are not responsible for major scattering. The grain size of the films is not expected to be very small as the full width at half the maximum of the x-ray diffraction peaks is also small. Plan-view samples of thermoelectric thin films on mica, examined by TEM and shown in Fig. 6, illustrate that the films are extremely well textured with preferred growth direction along the c axis. The grain size of the films is 1–2 μm and thus the grain boundaries could not be responsible for scattering. Point defects and nonstoichiometric regions are considered responsible for scattering. Annealing of the films is responsible for the reduction in point defects and thus an improvement in the mobility of the carriers.

Downloaded 24 Nov 2003 to 160.91.48.189. Redistribution subject to AIP license or copyright, see http://ojps.aip.org/japo/japcr.jsp

TABLE III. Highest values of Seebeck coefficient, carrier mobility, and carrier concentration in the thermoelectric films.

Parameter	Substrate	*n* type	*p* type
Highest α (μV/K)	Mica	−74.15	86.64
	AlN/Si(100)	−166.37	142.2
	AlN/Si(111)	−154.69	124.34
Highest μ (cm^2/V s)	Mica	40.42	28.89
	AlN/Si(100)	65.37	35.33
	AlN/Si(111)	68.84	19.41
Highest carrier concentration (cm^{-3})	Mica	1.38×10^{20}	3.41×10^{19}
	AlN/Si(100)	2.15×10^{20}	1.02×10^{20}
	AlN/Si(111)	3.59×10^{20}	4.46×10^{19}

The larger Seebeck values obtained for the films deposited on mica substrates are about 2.5 times lower than that for the bulk materials.[16,17] The lower values of the Seebeck coefficient for the films deposited on mica are related to nonstoichiometry, nonuniform composition, and defects in the films. The improved values of the Seebeck coefficient from the films on AlN/Si were obtained when lower density plasma was generated and particulate density was reduced. Also, an annealing step was used to relieve the large thermal stresses, homogenize the composition, and reduce point defects. The large difference in the thermal expansion coefficient of the thermoelectric films and that of the mica or AlN/Si substrate is also expected to introduce interfacial defects. The thermal expansion coefficient of Bi_2Te_3-based compounds (20×10^{-6}/K) and that of AlN/Si (2×10^{-6}/K) is responsible for large tensile thermal strains in the thin film upon cooling.

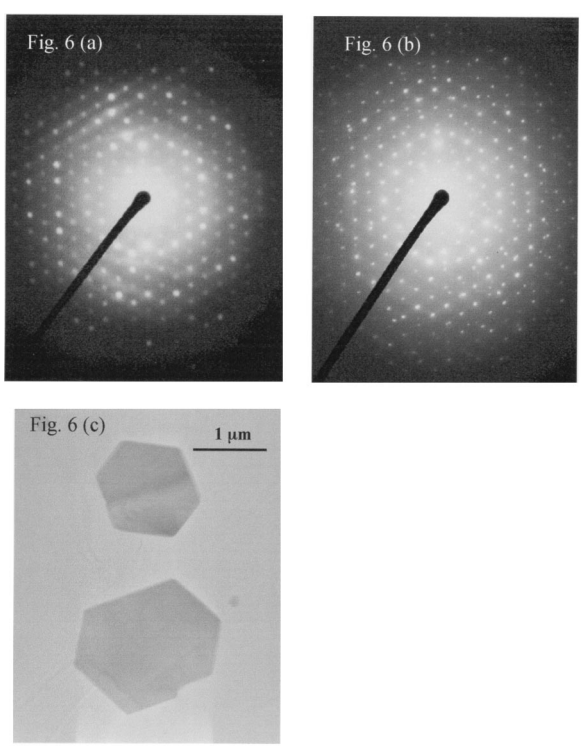

FIG. 6. (a) SADP obtained from the mica sheet used as a substrate material. (b) SADP obtained on the thermoelectric thin films deposited on mica substrates. (c) Bright-field TEM image obtained on thermoelectric thin films illustrating the presence of hexagon shaped crystallites.

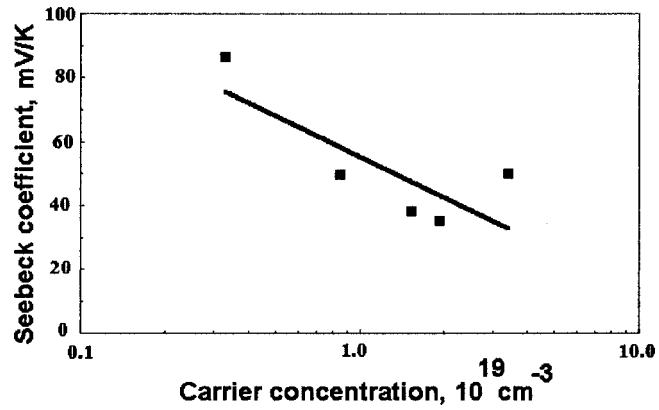

FIG. 7. Variation of thermoelectric power with carrier concentration for *p*-type films deposited on mica.

The values of the Seebeck coefficient are shown as a function of the carrier concentration in Figs. 7 and 8 for films on mica and Figs. 9 and 10 for films on AlN/Si. The observed increase in the Seebeck coefficient (α) with decreasing carrier concentration is expected from the following relation for α[18]

$$\alpha_{n,p}=\pm(k/q)[r+2+\ln(N/n)], \tag{1}$$

with the negative sign for *n*-type and positive sign for *p*-type thermoelectric compounds, k is the Boltzmann's constant, r is the scattering parameter, n is the carrier concentration, N is the density of states at the band edge given by $2(2\pi m^*kT)^{3/2}/nh^3$, h is the Planck's constant, m^* is the effective mass of the charge carriers, and T is the temperature. In the presence of impurities, the scattering parameter r is equal to 2, while $r=0$ for the atomic lattice. This result is found to follow with some deviation in the films on all of the

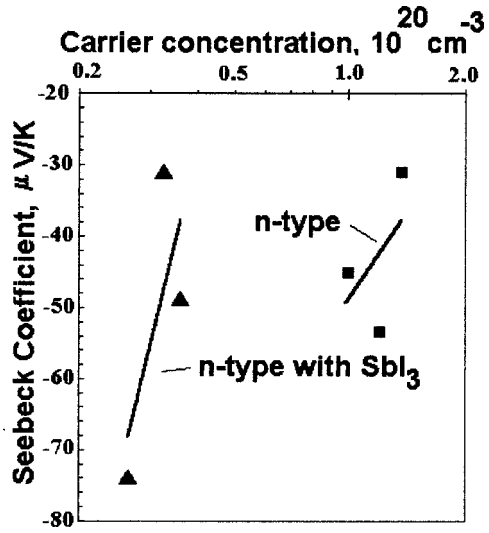

FIG. 8. Variation of thermoelectric power with carrier concentration for *n*-type films deposited on mica.

Downloaded 24 Nov 2003 to 160.91.48.189. Redistribution subject to AIP license or copyright, see http://ojps.aip.org/japo/japcr.jsp

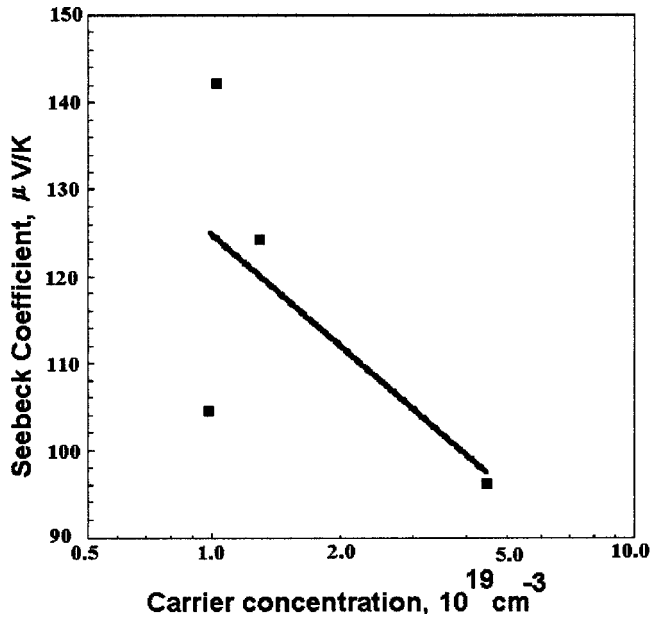

FIG. 9. Variation of thermoelectric power with carrier concentration for *p*-type films deposited on AlN.

substrates, as shown by the results in Figs. 7 to 10. The large variation in the Seebeck coefficient shown in Fig. 7 for a similar concentration of carriers for *p*-type films deposited at different temperatures is associated with the large differences in the mobility. The *p*-type films were deposited from a target that was compacted and sintered from powder leading to nonstiochiometry and defects in the films. The $\alpha_{n,p}$ versus $\ln(N/n)$ relation emphasizes that the carrier concentration, *n*, and density of states, *N*, are important factors in addition to the scattering parameter, *r*, that determine the thermoelectric properties of the films. In order to further improve the values of Seebeck coefficient, targets, with different concentrations

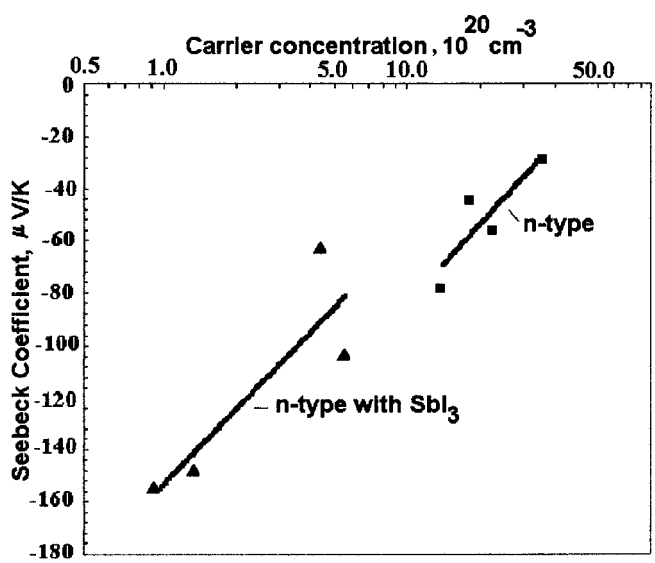

FIG. 10. Variation of thermoelectric power with carrier concentration for *n*-type films deposited on AlN.

TABLE V. Values of ZT reported[a] for *n* and *p*-type target materials.

Target composition	α (μV/K)	ρ(Ω cm)	K (assumed) (W/cm K)	ZT
p—$Bi_{0.5}Sb_{1.5}Te_3$	232.2	0.0017	0.014	0.68
n-$(Bi_2Te_3)_{90}(Sb_2Te_3)_5(Sb_2Se_3)_5$ (SbI_3 doped)	−206	0.0011	0.012	0.96

[a]See Ref. 17.

of dopants could be attempted as dopant evaporation in the plume, can significantly alter the stoichiometry and thus impact the carrier density in the thin films.

The use of thermoelectric films for cooling electronic devices is measured by the thermoelectric figure of merit, *Z*, given by $Z=\alpha^2/\rho K$, where *K* is thermal conductivity and the other parameters are already defined. The thermoelectric compounds possess low thermal conductivity whereas the substrates used in this investigation are good thermal conductors. The thermal conductivity of the thin films is smaller than that of the bulk thermoelectric compounds. Phonon scattering at the grain boundaries, defects in the films, and interfaces is known to reduce the thermal conductivity below that of the bulk. We have assumed the thermal conductivity values of 0.003 W/cm K and 0.004 W/cm K for the n and p type, respectively, and these values are smaller by a quarter from the bulk. The values of figure of merit, *ZT*, for the target and films at 300 K are shown in Tables IV and V respectively. The ZT values of 0.05 and 0.17 for the *p*- and *n*-type for films on mica, respectively, are quite low. However, the ZT value for the *n*- and *p*-type films on AlN/Si was found to be 0.25 and 0.08, respectively. The value of 0.25 for the *n*-type film on AlN/Si is less than that obtained for optimized bulk materials ($ZT\approx 0.96$). The large variation in the value of ZT, with a carrier concentration for *n*-type films on mica, is associated with one particular film that exhibited a higher mobility of carriers and, thus, a higher Seebeck coefficient and a higher value of ZT than the other. The value of figure of merit is reduced with decreasing thickness of the films below 5 μm.[1] The thickness of the films deposited for 1 h is 1.5 μm and, therefore, an increase in thickness by a longer deposition time is expected to further improve the ZT value.

More importantly, maximizing the value of ZT is equivalent to doing the same with the parameter $N_o m^{*3/2}\mu/K_L$, where m^* is the effective mass of the majority charge carrier, N_o is the number of equivalent parabolic bands, K_L is the lattice thermal conductivity, and μ is the carrier mobility.[18,19] The values of ZT for all of the films have been shown as a function of the mobility μ and the carrier concentration *n* in Figs. 11–14. These results indicate

TABLE IV. Highest values of ZT obtained on *n* and *p*-type films.

Films	α (μV/K)	ρ(Ω cm)	K (assumed) (W/cmK)	ZT
p type on mica	86.64	0.0104	0.003	0.05
p type on AlN	142.2	0.0194	0.004	0.08
n type on mica	−53.47	0.001 71	0.003	0.17
n type on AlN	−154.69	0.009 48	0.003	0.25

Downloaded 24 Nov 2003 to 160.91.48.189. Redistribution subject to AIP license or copyright, see http://ojps.aip.org/japo/japcr.jsp

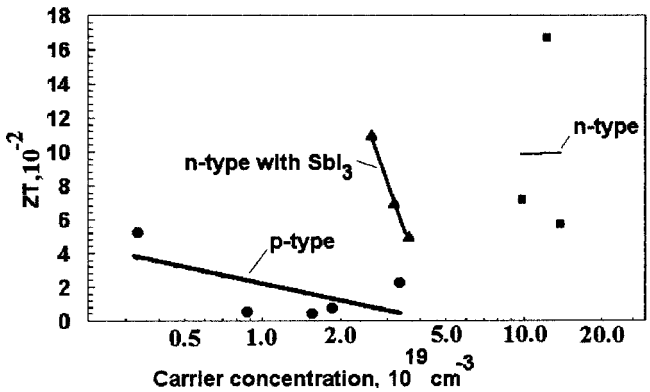

FIG. 12. *ZT* vs carrier concentration for thermoelectric films deposited on mica.

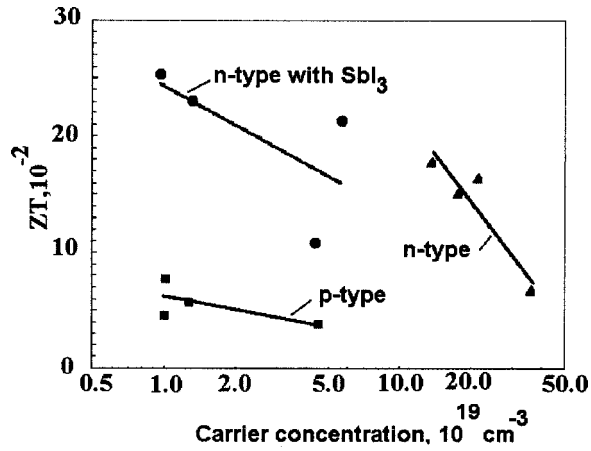

FIG. 14. *ZT* vs carrier concentration for thermoelectric films deposited on AlN.

that higher carrier mobility with optimized carrier concentration is necessary to obtain thin films with a higher *ZT* value. The values of mobility in the thermoelectric thin films deposited on mica and AlN/Si substrates were smaller compared to the values in the bulk.[16,17] The lower values of mobility in the films could be attributed to scattering by point defects and impurities. Recombination centers and traps in addition to impurity scattering are also present at the grain boundaries. Though it is seen that the films deposited from the *n*-type $(Bi_2Te_3)_{90}(Sb_2Te_3)_5(Sb_2Se_3)_5$ (with 0.13 wt % SbI_3) target showed a higher Seebeck value as well as a higher mobility, further improvement and higher *ZT* value could be achieved with larger thickness, better stoichiometry, uniform composition, and a reduction in defects. A dramatic improvement in the value of *ZT* through an increase in N_o by the formation of nanocrystalline films is already reported.[20–22]

V. CONCLUSIONS

The following conclusions are reached from the deposition and characterization of thermoelectric *p*- and *n*-type films by PLD on substrates of mica and AlN/Si:

(1) X-ray diffraction, scanning electron microscopy, TEM showed that the textured growth of thermoelectric films on AlN/Si and mica substrates could be achieved by using PLD. The films showed uniform thickness and high crystalline quality with a preferred (00*n*) alignment with the substrates.

(2) Congruent transfer of the target composition to the thin films was achieved with lower laser fluence. It was found that films with improved crystallinity and thermoelectric characteristics could be deposited at temperature between 300 to 350 °C.

(3) Improved *n*-type films on AlN/Si substrates were obtained from a $(Bi_2Te_3)_{90}(Sb_2Te_3)_5(Sb_2Se_3)_5$ target doped with 0.13 wt % of SbI_3 and showed a *ZT* value of 0.25. The *p*-type films deposited from a $Bi_{0.5}Sb_{1.5}Te_3$ target, however, showed a lower value of 0.08. The values of Seebeck coefficient were lower and that of the electrical resistivity higher from the films compared to the same parameters from the bulk targets. These results indicate that the carrier concentration is higher than the optimum value and the mobility of the charge carriers is lower.

(4) Thermoelectric properties in the films could be improved by the better control of stoichiometry, increase in film thickness, and minimization of the volume fraction of particulates, pores, and atomic level point defects.

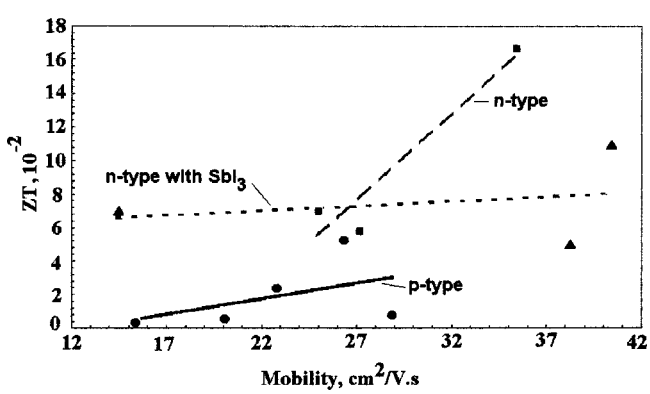

FIG. 11. *ZT* vs carrier mobility for thermoelectric films deposited on mica.

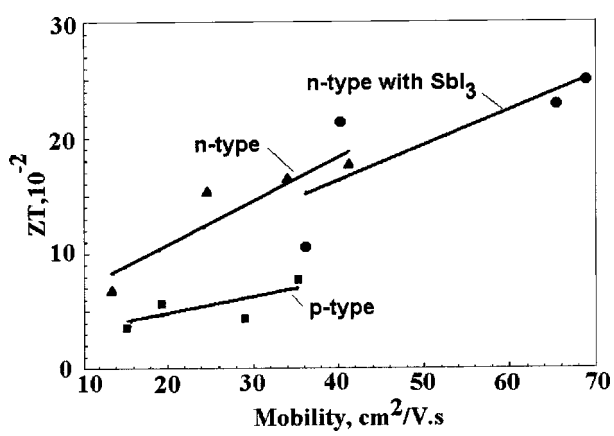

FIG. 13. *ZT* vs carrier mobility for thermoelectric thin films deposited on AlN.

Downloaded 24 Nov 2003 to 160.91.48.189. Redistribution subject to AIP license or copyright, see http://ojps.aip.org/japo/japcr.jsp

(5) The present effort has illustrated the use of AlN/Si, an efficient heat spreader, also as a favorable substrate material for the deposition of thermoelectric films.

ACKNOWLEDGMENTS

The authors wish to thank Professor W. A. Jesser of the University of Virginia and Dr. J. W. Sharp of Marlow Industries Inc., for valuable discussions and for providing the *n*-type targets. This research is supported in part by South Eastern Universities Research Association and the NSF. Also, the authors wish to acknowledge the travel support provided by Oak Ridge Associated Universities. Part of this research is sponsored by the Assistant Secretary for Energy Efficiency and Renewable Energy, Office of Transportation Technologies, as part of the High-Temperature Materials Laboratory User Program, ORNL, managed by UT-Battelle, LLC, for the U.S. Department of Energy under Contract No. DE-AC05-000R22725.

[1] J. R. Weise and L. Muller, J. Phys. Chem. Solids **15**, 13 (1960).
[2] J. W. Vandersande and J.-P. Fleurial, *Proceedings of the 15th International Conference on Thermoelectrics*, Pasadena, CA (1996), pp. 252–255.
[3] F. Völklein *et al.*, Thin Solid Films **187**, 253 (1990).
[4] A. Mzerd *et al.*, J. Mater. Sci. Lett. **13**, 301 (1994).
[5] M. Stölzer, V. Bechstein, and J. Meusal, *Proceedings of the 15th International Conference on Thermoelectrics*, Pasadena, CA (1996), pp. 422–424.
[6] A. Dauscher, A. Thomy, and H. Scherrer, Thin Solid Films **280**, 61 (1996).
[7] D. B. Chrisey and G. K. Hubler, eds., *Pulsed Laser Deposition of Thin Films* (Wiley, New York, 1994).
[8] J. W. Horwitz and J. A. Sprague, in *Pulsed Laser Deposition of Thin Films*, edited by D. B. Chrisey and G. K. Hubler (Wiley, New York, 1994), p. 229.
[9] R. E. Muenchausen and X. D. Wu, in *Pulsed Laser Deposition of Thin Films*, edited by D. B. Chrisey and G. K. Hubler (Wiley, New York, 1994), p. 357.
[10] D. K. Fork in *Pulsed Laser Deposition of Thin Films*, edited by D. B. Chrisey and G. K. Hubler (Wiley, New York, 1994), p. 393.
[11] R. E. Leuchtner and K. S. Grabowski, in *Pulsed Laser Deposition of Thin Films*, edited by D. B. Chrisey and G. K. Hubler (Wiley, New York, 1994), p. 473.
[12] S. B. Ogale in *Pulsed Laser Deposition of Thin Films*, edited by D. B. Chrisey and G. K. Hubler (Wiley, New York, 1994), p. 567.
[13] J. D. Plummer, M. D. Deal, and P. B. Griffin, *Silicon VLSI Technology* (Prentice–Hall, Englewood Cliffs, NJ), pp. 539–551.
[14] K. Jagannadham, J. Vac. Sci. Technol. A **17**, 373 (1999).
[15] J. C. Tedenac, S. Dal Corso, A. Hadioux, S. Charar, and B. Liautard, Mater. Res. Soc. Symp. Proc. **545**, 93 (1998).
[16] M. H. Ettenberg, W. A. Jesser, and F. D. Rosi, *Proceedings of the 15th International Conference on Thermoelectrics Proceedings*, Pasadena, CA (1996), pp. 52–56.
[17] J. Seo, K. Park, C. Lee, and J. Kim, Mater. Res. Soc. Symp. Proc. **478**, 127 (1997).
[18] A. F. Ioffe, *Semiconductor Thermoelements and Thermoelectric Cooling* (Infosearch Limited, London, 1957), p. 20.
[19] G. D. Mahan, B. C. Sales, and J. W. Sharp, Phys. Today **50**, 42 (1997).
[20] L. D. Hicks and M. S. Dresselhaus, Phys. Rev. B **47**, 12727 (1993).
[21] R. Venkatasubramanian, E. Silvola, T. Colpitts, and B. O'Quinn, Nature (London) **413**, 597 (2001).
[22] T. C. Harman, P. J. Taylor, D. L. Spears, and M. P. Walsh, J. Electron. Mater. **29**, 1 (2000).

Downloaded 24 Nov 2003 to 160.91.48.189. Redistribution subject to AIP license or copyright, see http://ojps.aip.org/japo/japcr.jsp